Supplementary Material: An examination of beta dose attenuation effects in coarse grains located in sliced samples

I.K.Bailiff

SM1. Radiation transport simulations

SM1.1 MCNP Configuration

The dosimetry models were constructed for use with the general-purpose radiation transport code MCNP, initially version 5 (Monte Carlo N-particle Transport Code; Forster et al., 2004) and more recently version 6 (Goorley et al., 2012). The condensed-history electron transport algorithms incorporated in the Integrated Tiger Series (ITS 3.0; Halblieb and Mellhorn, 1984) were employed in the simulations in view of the issues of the handling of electron transport simulation in the default mode of MCNP (Schaart et al., 2002; Reynaert et al., 2002; Nathan et al., 2003). In terms of the calculation of electron transport described here, version 5 of MCNP is expected to provide output equivalent to MCNP version 4 as used by Nathan et al. (2003) and Aznar et al. (2003), and the ITS ACCEPTP code used by Brennan (2003). MCNP calculates the energy absorbed in the detector volume per unit activity of the source, and this quantity was used to calculate, using the coefficients discussed in Section 2.4, the dose rate to the detector volume as specified in each model. Simulations were performed for a number of particle histories sufficient to obtain a precision of 1-2% achieved in most cases, after 10^5-10^7 histories per simulation, but requiring up to 10^{10} (~1k cpu-h) histories where the detector volume was small. Some simulations were repeated with different random number generator starting values to check the consistency of the variation in the calculated dose coefficients with the parameter uncertainty computed by MCNP.

SM1.2 Model source terms

The beta particle energy spectra for the lithogenic sources were obtained from the MIRD (Medical Internal Radiation Dose) database and the NUDAT 2 program (www.nndc.bnl.gov), and also included data from the RADAR database (www.doseinfo-radar.com). For sources of natural uranium and thorium, a composite beta spectrum was constructed with appropriately weighted contributions from each beta emitting member of the decay series, including internal conversion electrons. In the case of ^{40}K there are differences in the values of the average beta decay energy for ^{40}K given in various nuclear databases. The spectrum presented in the RADAR database is the most consistent with our calculation of the spectrum (Slim, pers. comm.) using an end-point energy of 1.311 MeV and a third forbidden unique spectral shape factor (Evans, 1955) which yield an average energy of 585 keV.

SM2. Total dose rate assessment

The total dose rate to the volume of a detector grain remaining in the sliced sample was calculated using a formulation based on that described previously (Bailiff, 2006). For the n^{th} detector grain in a dry medium the total dose rate, $\dot{D}^{tot}_{SGn}$, is expressed as the sum of dose rate contributions arising from sources external to and within the grain:

$$\dot{D}^{tot}_{SGn} = \{((a'\dot{D}^{i}_{\alpha} + a\dot{D}^{m}_{\alpha})\,(V_{TG}\text{-}V^{i}_{TG})/V_{TG}) + \phi_T\dot{D}^{i}_{\beta}\} + \{(1\text{-}\phi_T)\dot{D}^{m}_{\beta} + \dot{D}_{\gamma} + \dot{D}_{c}\}, \qquad \text{(SM1)}$$

(Internal grain sources / External grain sources)

where: the terms within the first and second curled brackets corresponds to internal grain sources and external matrix sources respectively; the dose rate term $\dot{D}$ has subscripts denoting radiation type (α, β, γ and cosmic) and superscripts *i* and *m* to indicate the internal grain or external matrix sources; *a* and *a*' are coefficients to account for alpha efficiency (*a*, internal grain sources) and, also, irradiation geometry (*a*', external sources); V_{TG} and V^{i}_{TG} are the volumes of the truncated grain and the inner grain volume of radius ($R\text{-}\alpha_R$) not penetrated by alpha irradiation respectively; the gamma and cosmic dose-rates correspond to the average within the sample volume under examination. The general formulation of the total dose rate to a truncated grain given in Eqn SM1 assumes a distribution of sources that is uniform within the infinite medium volume (IMV) surrounding the grain (i.e., within a radius of ~3 mm) and within the grain, if present.

SM2.1 External alpha dose – effect of truncation

Truncation also affects the contribution of the external alpha dose and, for the purposes of estimating the total dose rate to single grains, its variation with truncation height was estimated using a simplified geometric approach (Bailiff, 2006). The volume of the alpha-dosed material, taken to be an outer shell of 20 μm thickness, was expressed as a fraction of the truncated grain volume below the surface, F_{VT}, and as the fraction for a whole grain, F_{WG}, which reflects the change in the proportion of alpha dose with degree of truncation. For the range of grain sizes considered here (R_S=250-1000 μm), the ratio F_{VT}/F_{WG} was found not to be strongly dependent of the value of the shell thickness, and consequently the use of an arbitrary penetration depth was judged not to be a critical factor. The value of the quotient, F_{VT}/F_{WG}, calculated for R_{WG} = 250, 500 and 1000 μm (Fig. SM3) shows little change with truncation height for the base section, but there is a substantial increase for the cap section, with up to a six-fold change for a 1000 μm radius grains giving rise to a higher contribution to the total dose rate from the alpha component. Since the alpha dose rate contribution to the base section is

generally less than 5% of the total rate for coarse grains within the size range considered here, the approximations made using this approach are not expected to give rise to large errors in the assessment of the total dose rate. However, more detailed calculations (Brennan et al., 1991) and modelling of the type performed previously by Brennan (2006) would be needed in the case of smaller grains (e.g., <100 μm).

SM3. Spherical source - dose profile

Radiation transport simulations performed with a spherical shell model (e.g., Janicki and Seuntjens, 2004) can be used to calculate, for a sphere containing a uniform distribution of sources, the radial dependence of dose within the sphere and extending into the surrounding medium (Fig. SM4) which is related to the DPK, F(s). As discussed in the main text, the integration of Eqn 1 over a spherical segment is strongly weighted by a volumetric factor, the general form of which is similar to that shown in Fig. SM3. The latter represents the variation in fractional volume of the outermost shell (of thickness 20 μm) of the truncated sphere with surface radius, R_s.

Additional References

Aznar, M.C., Nathan, R.P., Murray, A.S., Bøtter-Jensen, L., 2003. Determination of differential dose rates in a mixed beta and gamma field using shielded Al_2O_3:C: results of Monte Carlo modelling. Radiat. Meas. 37, 329-334.

Brennan, B.J., Lyons, R.G., Philips, S.W., 1991. Attenuation of alpha particle track dose for spherical grains. Nucl. Tracks Radiat. Meas. 18, 249-253.

Brennan, B.J., 2006. Variation of the alpha dose rate to grains in heterogeneous sediments. Radiat. Meas. 41, 1026-1031.

Evans, R.D., 1982. The Atomic Nucleus. McGraw Hill, New York.

Halblieb, J.A., Mehlhorn, T.A., 1984. ITS: The integrated TIGER series of coupled electron/photon Monte Carlo transport codes. Sandia report SAND 84-0573, Sandia National Laboratories, New Mexico.

Janicki, C., Seuntjens, J., 2004. Accurate determination of dose-point-kernel functions close to the origin using Monte Carlo simulations. Medical Physics 31, 814-818.

Reynaert, N., Palmans, H., Thierens, H., Jeraj, R., 2002. Parameter dependence of the MCNP electron transport in determining dose distributions. Medical Physics 29, 2446-2454.

Schaart, D.R., Jansen, J.Th.M., Zoetelief, J., de Leege, P.F.A., 2002. A comparison of MCNP4C electron transport with ITS 3.0 and experiment at incident energies between 100 keV and 20 MeV; influence of voxel size, substeps and energy indexing algorithm. Phys. Med. Biol. 47, 1459-1484.

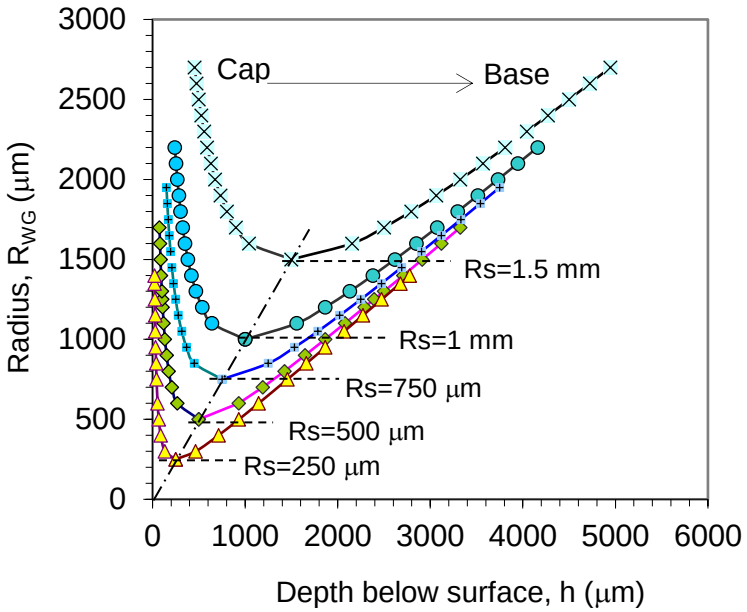

Figure SM1
Relationship between the radius R_{WG} of spheres, representing parent grains, and the depth of truncation, h, for different values of the surface radius, R_S. Cutting the spheres at height h. divides the sphere into cap and base sections as shown in the figure, with the base section being the larger of the two. The broken line intersecting the origin passes through the point of bisection of the spheres (R_{WG}=R_S).

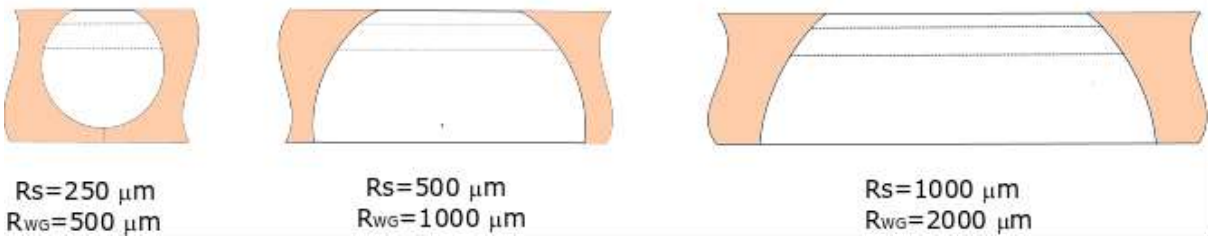

Figure SM2
Examples of slice cross sections showing the base sections of three truncated grains within a 1 mm-thick slice that present a surface radius, R_S, of 250, 500 and 1000 mm, where in each case the parent grain radius, R_{WG}, is $2R_S$. The boundaries of the layers L1 and L3 discussed in the main text are indicated by broken lines.

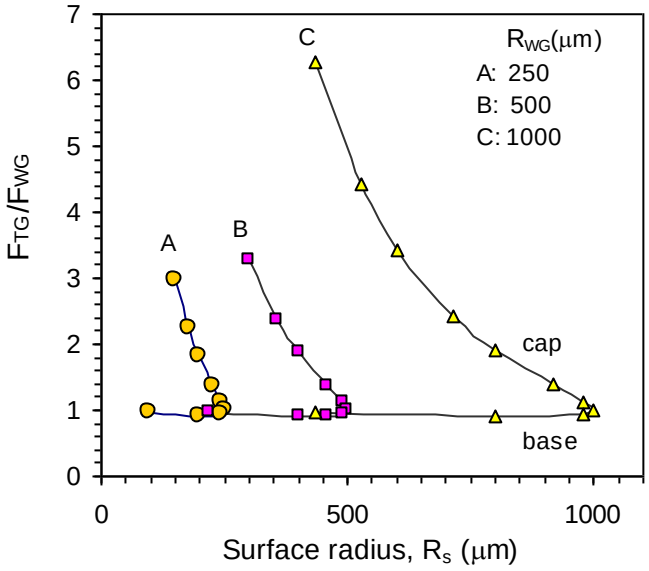

Figure SM3

Normalised fractional α-dosed volume, F_{TG}/F_{WG}, vs surface radius, R_S, of a truncated spherical grain for three sizes of parent grain (R_{WG}=250, 500 and 1000 μm), where the sources are external to the grain which is free of sources. F_{TG} =volume of the outer α particle penetrated layer (α_R=20 μm) of a truncated grain, expressed as a fraction of volume of the truncated grain and F_{WG} = the same for the parent grain.

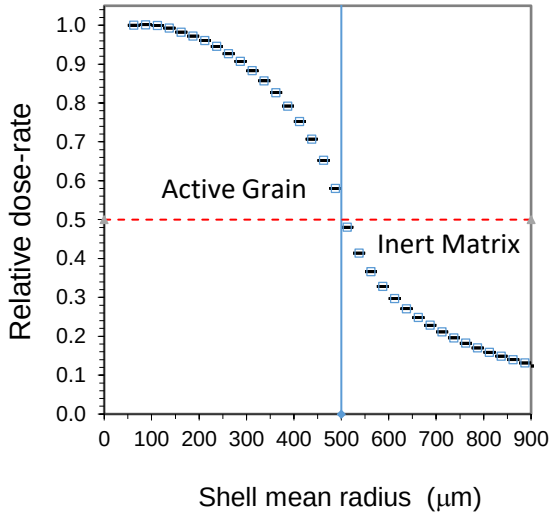

Figure SM4

Calculated dose rate profile for a sphere (R_{WG}=500 μm) composed of quartz containing a uniform distribution of ^{40}K sources and set in an inert quartz matrix. The radiation transport simulation model employed a spherical shell geometry (shell width = 25 μm), as widely adopted in the calculation of a dose point kernel.